Shear testing of stack bonded masonry

P.B. Lourenço[1†], J.O. Barros[2] and J.T. Oliveira[3]

1 Abstract

Stack bonded masonry is scarcely used in practice, except for aesthetic reasons. Nevertheless, a regular array of units allows to place reinforcement in the joints, which can be of major importance for masonry shell roofs, as proposed by Eladio Dieste. In order to contribute to the knowledge of the behavior of stack bonded masonry under shear loading, which seems not to have been addressed before, an experimental research program using the triplet test was carried out. The specimens incorporate aligned joints along two orthogonal axes, filled with micro-concrete. The main results of the experimental program are herein presented and discussed.

Keywords:

Masonry; Shear testing; Coulomb failure criterion; Dilatancy

2 Introduction

Eladio Dieste [1], (1917-2000), was a well-known Uruguayan engineer that designed a significant number of innovative curved masonry shells for roofs and walls. The orthogonal array of facing ceramic bricks provided the location for the placement of steel reinforcement, being simultaneously low-cost, aesthetically appealing and structurally efficient. The main difficulty of using similar approaches in developed countries is related to cost of formwork and manpower. Currently, several European institutions and private companies are involved in the development of an industrialized solution for short and medium span shell roofs, under European contract GROW-

[1] Associate Professor of Civil Engineering, University of Minho, Azurém, P – 4800-058 Guimarães, Portugal, Tel + 351 510 200, Fax +351 253 510217, E-mail pbl@civil.uminho.pt
[†] Corresponding Author
[2] Assistant Professor of Civil Engineering, University of Minho, Azurém, P – 4800-058 Guimarães, Portugal, barros@civil.uminho.pt
[3] PhD student, University of Minho, Azurém, P – 4800-058 Guimarães, Portugal, juliana@civil.uminho.pt

1999-70420 “ISO-BRICK”. The usage of stack bonded masonry, together with joints filled with micro-concrete, is uncommon and requires adequate experimental testing. In this paper, the behavior of such masonry under shear loading is characterized.

The failure behavior of masonry joints under shear, with moderate pre-compression levels, can be represented by the Coulomb friction law, which establishes a linear relationship between the shear stress τ and the normal stress σ, being given by

$$\tau = c + tan\phi \cdot \sigma \,. \tag{1}$$

Here, c represents the cohesion and $tan\phi$ is the tangent of the friction angle of the interface between unit and micro-concrete. For higher normal compressive stresses, the validity of the Coulomb failure is lost and crushing / shearing of the units, accompanied by cracking is found. In this case, a cap model can be adopted to represent failure of the combined joint – unit ensemble, see e.g. [2].

Another relevant feature of masonry joints is the so-called dilatancy angle ψ, which measures the volume change upon shearing. The ratio between the normal displacement u_n and the shear displacement u_s gives $tan\psi$, which can assume positive or negative values. Usually, the dilatancy angle is positive but tends to zero upon increasing shear displacement and increasing normal confining stress [3].

For the purpose of characterizing the behavior of masonry under shear, different test methods to determine the strength parameters c, $tan\phi$ and the volume parameter $tan\psi$ have been adopted by researchers, e.g. [3-9], see Figure 1.

All test methods fail to reproduce an absolutely uniform distribution of the normal and shear stresses, even if the triplet test has been adopted has the standard test in Europe, prEN 1052-3 – “Methods of test for masonry – Part 3: Determination of initial shear strength” [10]. Here, the testing method adopted is the triplet test proposed in EN 1052-4 – “Methods of test for masonry – Part 4: Determination of shear strength including damp proof course” [11], given the stacked nature of the masonry panels and the novel use of micro-concrete. In total, nine masonry specimens have been tested, in three series associated with three different normal pre-compression load levels. Additionally, the strength values of the masonry units and micro-concrete used for the joints have been also characterized.

3 Adopted Materials and Test Set-up

3.1 Materials Characterization

The clay units used in the masonry panels (produced and delivered in a single batch) have been produced especially for the current research project. The unit dimensions are 215mm (length), 100mm (width) and 65mm (height). The unit is hollow with two holes of 25mm × 25mm, in order to reduce the weight of the masonry shells.

The masonry joints have a thickness of 25 mm and are to be filled with micro-concrete, made using small aggregate size. Micro-concrete has been selected for the joint because, in the final masonry roof shells (not considered here), a top screed of concrete will be used for structural purposes. The masonry roof shells are to be reinforced with steel rebars in the joints, meaning that a special purpose concrete mix with a high slump is required. The adopted concrete composition consists of 360kg of cement, 615kg of gravel, 1208kg of sand, 174L of water and 3.60L of Superplastifier Rebuilt 1000, per m^3, which returns a slump of 160mm.

The strength properties of the masonry components are given in Table 1.

The compressive strength of the masonry units was obtained according to [12]. Due to the anisotropy associated with the extrusion process and firing, the uniaxial compression tests were carried out in two orthogonal directions, namely along the length (X direction) and height (Y direction) of the unit, as illustrated in Figure 2. In order to limit the restraining effect of the machine steel loading platens, full units have been used for testing in the X direction, while only half unit specimens were used for testing in the Y direction. The surface of all specimens was ground to ensure planarity of the loading faces.

All tests were carried out in dry specimens. The specimens were stored at constant temperature of 105ºC ±5ºC in stove, until constant mass was reached. A universal testing machine with a maximum loading capacity of 3000 kN was used in the tests. The values for the compressive strength of the units represent the average of eight specimens, indicating a 1:2.3 anisotropy due to the holes in the units and the extrusion process.

The (direct) tensile strength of masonry units was obtained carrying out direct tension tests with notched specimens, see [13] for details. The values for the tensile strength of the units represent, at least, the average of ten specimens, indicating a 1:2.0 anisotropy due to the holes in the units and the extrusion process.

The compressive strength of concrete at 28 days is the average of four results obtained in tests with cylindrical specimens (diameter of 150 mm and height of 300 mm), according to the recommendations of RILEM CPC4 [14]. The

(flexural) tensile strength of concrete at 28 days is the average of four results obtained on three point bending tests with notched concrete beams, according to the recommendations of RILEM FMC1 [14].

3.2 Description of the Test Set-up

The specimens consist of three masonry courses subjected to a vertical pre-compression load, see Figure 2b. The top and bottom masonry courses are kept under constant pressure while a horizontal load is applied in the middle masonry course. Eventually this course slides, providing the value of the shear strength of the joints. Therefore, two joints are tested simultaneously.

In order to define the cohesion and the friction angle of the joints, three different pre-compression stress levels were adopted, namely 0.2N/mm^2, 0.6N/mm^2 and 1.0N/mm^2. These stress levels were kept constant during the complete tests duration. For each pre-compression stress level, three panels were tested, resulting in a total of nine tests. The specimens were divided in three series: series 1 for a pre-compression level of 0.2N/mm^2 (panels B1 to B3), series 2 for a pre-compression level of 0.6N/mm^2 (panels B4 to B6) and series 3 for a pre-compression level of 1.0N/mm^2 (panels B7 to B9).

Two horizontal rigid supports restricted the movement of the top and bottom courses of the panel. These supports are pinned and cover the full height of the course in order to minimize any bending effect of the panel. The horizontal and vertical loading system consisted of two independent actuators. The horizontal actuator was applied directly on the middle course and the vertical actuator was applied on a steel beam, so that the load could be evenly distributed in the panel.

Initially, the vertical compressive load was applied by means of the vertical hydraulic actuator under force control at a rate of 10kN per minute. The maximum loading capacity of the vertical actuator is 50kN. Subsequently, the vertical load was kept almost constant, as shown in Figure 3, which illustrates the time history of the vertical load for each panel series. It can be observed that the vertical load was kept approximately constant during the test duration, with the exception of some sudden load variations due to the geometrical irregularities of the failure surfaces of the joints. The irregularities have imposed a minor ascending movement of the top steel beam, inducing the temporary increase of the vertical load during testing.

After the application of the selected pre-compression level, the horizontal load was applied by imposing small displacement steps with a hydraulic actuator of a maximum loading capacity equal to 250kN. The horizontal shear load, measured with a load cell, was applied with a velocity of 20μm / second.

The displacements of the panel were recorded with eight linear voltage displacement transducers (LVDTs). Four LVDTs were placed on the front of the specimens to measure the displacements in the horizontal direction and three LVDTs were placed on the back of the specimen to measure the vertical displacements. As stated above, one LVDT was located at the horizontal actuator so that the test could be carried out under displacement control. The positions of the LVDTs are illustrated in Figure 4.

4 Obtained Experimental Results

4.1 Series 1 – Panels B1, B2 and B3

Figure 5a shows the relation between the shear load and the horizontal displacement at the joints for series 1. Here, the horizontal displacement represents an average of the measurements recorded using LVDTs 1-4 (the average of LVDTs 1-3 measurements was averaged with the measurement recorded in LVDT 4), placed on the horizontal direction. Figure 5b illustrates the relation between the horizontal displacements of the two horizontal joints. Here, the bottom joint value is the average of the recordings from LVDTs 1-3 and the top joint value is the recording of LVDT 4.

Finally, Figure 6 presents the failure mode of the panels. It is noted that the variation of the recordings amongst LVDTs 1-3, located at the bottom joint, is usually minimal for all specimens. The sole exception is the case of complex failure modes that include head joints or diagonal cracks through the units, e.g. Panel B2.

The post-peak response of panel B1 could not be recorded but the post-peak response of panels B2 and B3 could be recorded until termination of the test.

Panel B1 collapse exhibits a stepped crack at the bottom joint and minor diffused cracked at the top joint. This indicates a probable displacement at the right top support that lead to minor sliding of the top joint. The collapse load of this test was similar to the other two tests, which indicates that both joints effectively slide.

In panel B2, the cracks deviated from the horizontal joints and progressed through the units and head joints. This can be due to the presence of firing cracks in the joints and deficiently filled head joints. The existence of gravel in the crossed joint can also preclude the crack propagation along the interface. This peculiar shape of collapse is stressed

in Figure 5b, where the vertical line for panel B2 indicates that no average horizontal displacement in the bottom joint could be recorded. This also indicates that the use of an average horizontal displacement in Figure 5a is debatable, for this particular panel.

The results for Panel B3 in terms of force-displacement diagram are coherent and follow the expected pattern. The residual plateau found in the response is associated with the friction of the joint. Nevertheless, a sudden increase of strength is observed at an average displacement of 2.0mm. This corresponds to the sudden jump in the diagram of Figure 5b. It is believed that the different displacements in the top and bottom joint are related to interlocking associated with the gravel size and to movements in the lateral supports. This clearly demonstrates the complexity of the phenomena involved in the failure of the triplet test.

Finally, the failure modes illustrated in Figure 6 show a clear trend for the occurrence of stepped crack in the right side of the joints, in the intersection of horizontal and vertical joints. It is believed that this stepped crack is due to the triplet test set-up, which is known to induce rotation of the principal stresses in the joint near the left and right edges.

4.2 Series 2 – Panels B4, B5 and B6

Figure 7a shows the relation between the shear load and the horizontal displacement at the joints for series 2. Due to the higher pre-compression level, the maximum shear load was increased. Figure 7b illustrates the relation between the horizontal displacements of the two horizontal joints.

The results for Panel B4 in terms of force-displacement diagram are coherent and follow the expected pattern. This panel failed simultaneously in the top and bottom joints. The joints in Panels B5 and B6 have failed in a similar way. Initially, only one joint has failed but, upon reloading, a second crack developed at the non-cracked interface. This is clearly in agreement with the diagrams in Figure 7b, where it can be seen that sliding in the bottom joint is not accompanied with sliding in the top joint, until a significant relative displacement is found. In Panel B6, it can be observed that global softening only occurs once both top and bottom cracks are formed, at an average horizontal displacement equal to circa 1.3mm (or a displacement in the bottom joint of circa 2.6mm).

4.3 Series 3 – Panels B7, B8 and B9

Figure 8a shows the relation between the shear load and the horizontal displacement at the joints for series 3. Due to the higher pre-compression level, again the maximum shear load was increased. Figure 8b illustrates the relation between the horizontal displacements of the two horizontal joints.

The post-peak response of panel B7 could not be recorded but the post-peak response of panels B8 and B9 could be recorded until termination of the test. Panel B7 exhibited a full crack of the bottom joint at a load of 120kN. This crack resulted in a rigid body rotation between the top and bottom part. Panel B8 and Panel B9 exhibited different load-displacement diagrams. The response of Panel B9 follows the expected pattern whereas a very ductile response was found for Panel B8. The first crack occurred in the top joint, as it can be seen in Figure 8b.

4.4 Definition of the Joint Strength Parameters

Figure 9 shows the relation between the normal stress and the shear strength for all tests, as well as a linear regression carried out with the shear strength average for each series of tests. The correlation coefficient r^2 of the linear regression is 0.997, which indicates an excellent correlation.

The linear regression indicates a cohesion value c equal to 1.39 N/mm^2 and a tangent of the friction tangent $\tan\phi$ equal to 1.03, see eq. (1). In standard masonry, the value of the tangent of friction angle seems to range between 0.7 and 1.2, according to different combinations of units and mortars [3]. The value obtained can therefore be considered acceptable. It is also stressed that according to the European Norm EN1052-4 [11], the characteristic value of the initial shear strength or cohesion is only 80% of the experimental value, or 1.11 N/mm^2 in this case.

4.5 Evaluation of the dilatancy

The relation between the vertical and the horizontal displacement is termed dilatancy. This quantity measures the uplift of one unit over the other upon shearing. It is known that the dilatancy decreases under increasing pre-compression levels. Additionally, dilatancy decreases to zero under increasing shearing displacement due to the smoothing of the sheared surfaces.

Figure 10 illustrates the measured dilatancy for panel B3, which is the first panel with recorded significant horizontal displacements. The figure seems to demonstrate that a zero dilatancy is also retrieved for the micro-concrete joints adopted in this case. The complete results for all tests are given in [15].

It is further noted that the given displacements were calculated using the average of displacements recorded by LVDTs 1, 3 and 4 (horizontal displacement) and LVDTs 5, 6 and 7 (normal displacement). The selected horizontal LVDTs (1, 3 and 4) were located on the opposite side of the panel associated with vertical LVDTs (5, 6 and 7). In such a way, the horizontal and vertical displacements were measured in the same location.

5 Conclusions

The triplet test was used successfully to assess the shear behavior of stack bonded masonry with micro-concrete joints. Standard masonry bond is the running bond, which results in discontinuous vertical joints. It is important to stress that the masonry panels studied in this paper had continuous vertical joints, just because they will be used to build reinforced masonry shells. Typical failure modes have been obtained and the shear strength seems to adequately follow Coulomb friction law. Therefore, both the use of a stacked configuration and the use of micro-concrete for the joints are acceptable.

The mechanical strength parameters that characterize the interface of the joints is a cohesion c of 1.39 N/mm^2 and a tangent of the friction angle $\tan\phi$ of 1.03. According to [11], the characteristic value of the cohesion c is 1.11 N/mm^2.

It was also found that the dilatancy of the masonry micro-concrete joints, in the stack bond configuration, is similar to standard masonry. In particular, dilatancy tends to zero upon progressive shearing.

Acknowledgements

The present work was partially supported by GROWTH project GROW-1999-70420 “ISO-BRICK” funded by European Commission.

References

1 . Dihel KN. Eladio Dieste reinforced brick structures. Ziegelindustrie International 1991; 44(10): 556-563.

2. Lourenço PB, Rots, JG. A multi-surface interface model for the analysis of masonry structures. J Engrg Mech, ASCE 1997; 123(7): 660-668.

3. Pluijm Rvd. Out of Plane Bending of Masonry Behaviour. PhD Thesis. Eindhoven University of Technology, The Netherlands, 1999.

4. Copeland RE, Saxer EL. Tests on structural bond of masonry mortars to concrete block. J ACI 1964; 61(11): 1411-1451.
5. Smith B S, Carter C. Hypothesis for shear failure of brickwork. J Struct Div, ASCE 1971; 97(4): 1055-1062.
6. Sinha BP, Hendry AW. Tensile strength of brick specimens. Proc Brit Ceram Soc 1975; 24, 91-100.
7. Hamid AA, Drysdale RG, Heidebrecht AC. Shear strength of concrete masonry joints. J Struct Div, ASCE 1979; 105(5): 1227-1240
8. Hofmann P, Stockl S. Tests on the shear-bond behaviour in the bed-joints of masonry. Mas Inter 1986; 9: 1-15.
9. Atkinson RH, Amadei BP, Saeb S, Sture S. Response of masonry and joints in direct shear. J Struc Engrg 1989; 115(9): 2276-2296
10. CEN. European norm for methods of test for masonry – Part 3: Determination of initial shear strength. prEN 1052-3, 1996.
11. CEN. European norm for methods of test for masonry – Part 4: Determination of shear strength including damp proof course. EN 1052-4, 2000.
12. CEN. European norm for methods of test for masonry units – Part 1: Determination of compressive strength. EN 772-1, 2000.
13. Almeida JC, Lourenço PB, Barros, JA. Characterization of brick and brick–mortar interface under uniaxial tension. In: Santos FA *et al.*, editors. Proceedings of 7th Int. Seminar on Structural Masonry, Brazil: CEFET-MG, 2002. p. 67-76.
14. RILEM. Technical recommendations for the testing and use of construction materials, 1994.
15. Oliveira JT, Lourenço PB, Barros JO. Shear testing of stack bonded masonry. Report no. 02-DEC/E-10. Universidade do Minho, Portugal, 2002. pp. 33.

Table 1 – Strength of masonry components, measured on the nominal unit size (in N/mm^2)

Material	*Compressive strength*	*Tensile strength*
Concrete	30.3	1.73
Unit (X direction)	71.8	3.50
Unit (Y Direction)	31.8	1.76

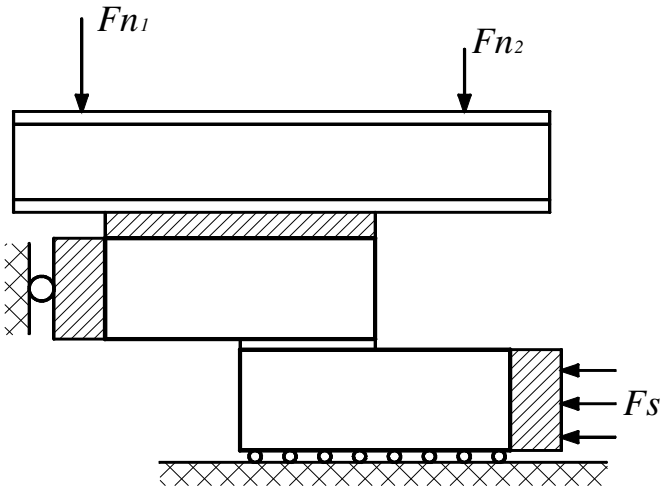

(a)

Figure 1 – Different types of shear tests: (a) couplet test, (b) van der Pluijm test [3] and (c) triplet test

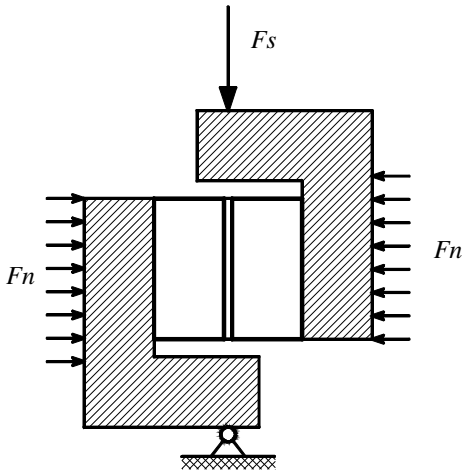

(b)

Figure 1 – Different types of shear tests: (a) couplet test, (b) van der Pluijm test [3] and (c) triplet test

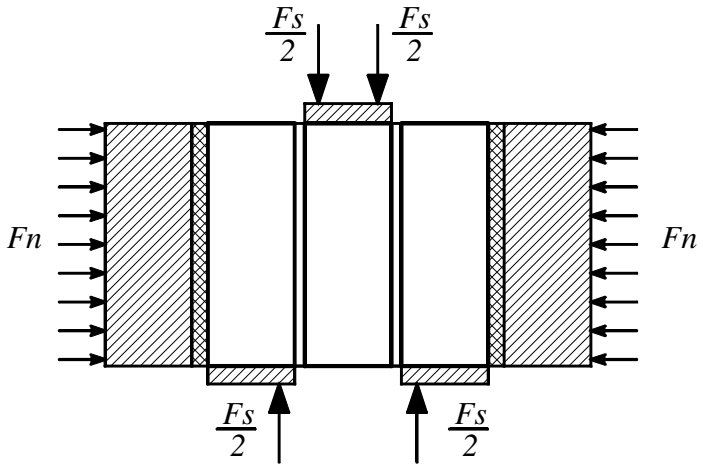

(c)

Figure 1 – Different types of shear tests: (a) couplet test, (b) van der Pluijm test [3] and (c) triplet test

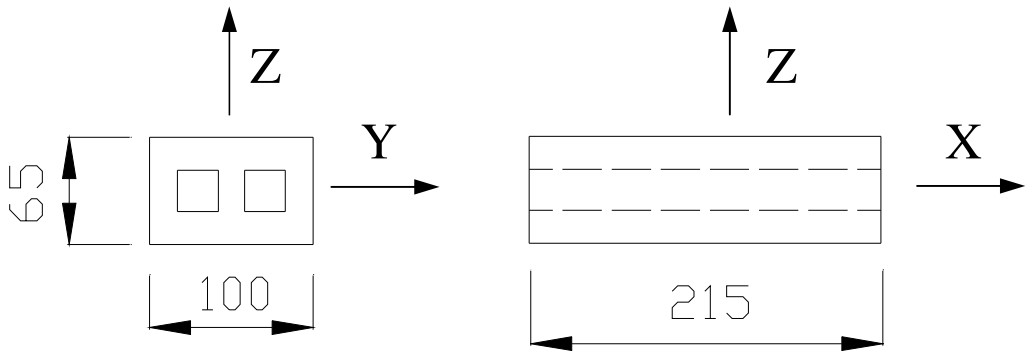

(a)

Figure 2 – Geometry of the (a) unit and (b) masonry specimens

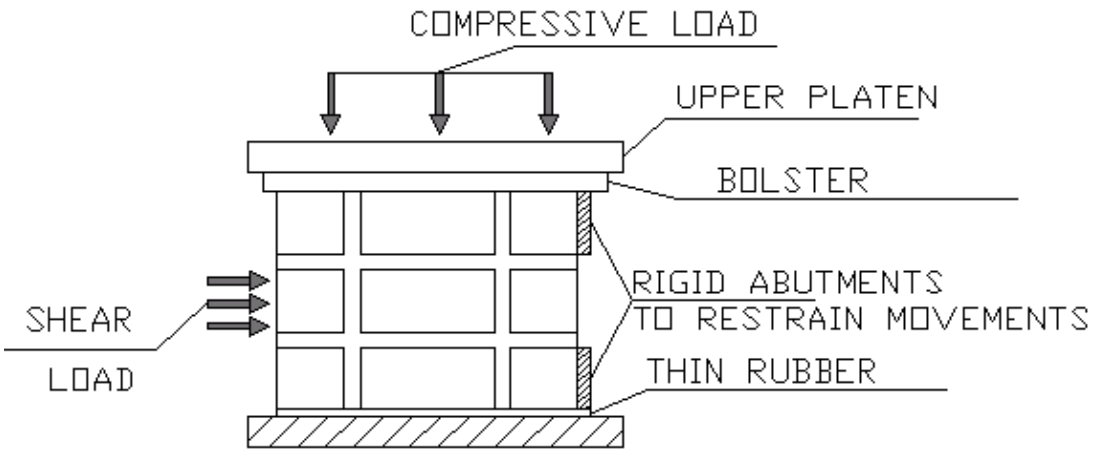

(b)

Figure 2 – Geometry of the (a) unit and (b) masonry specimens

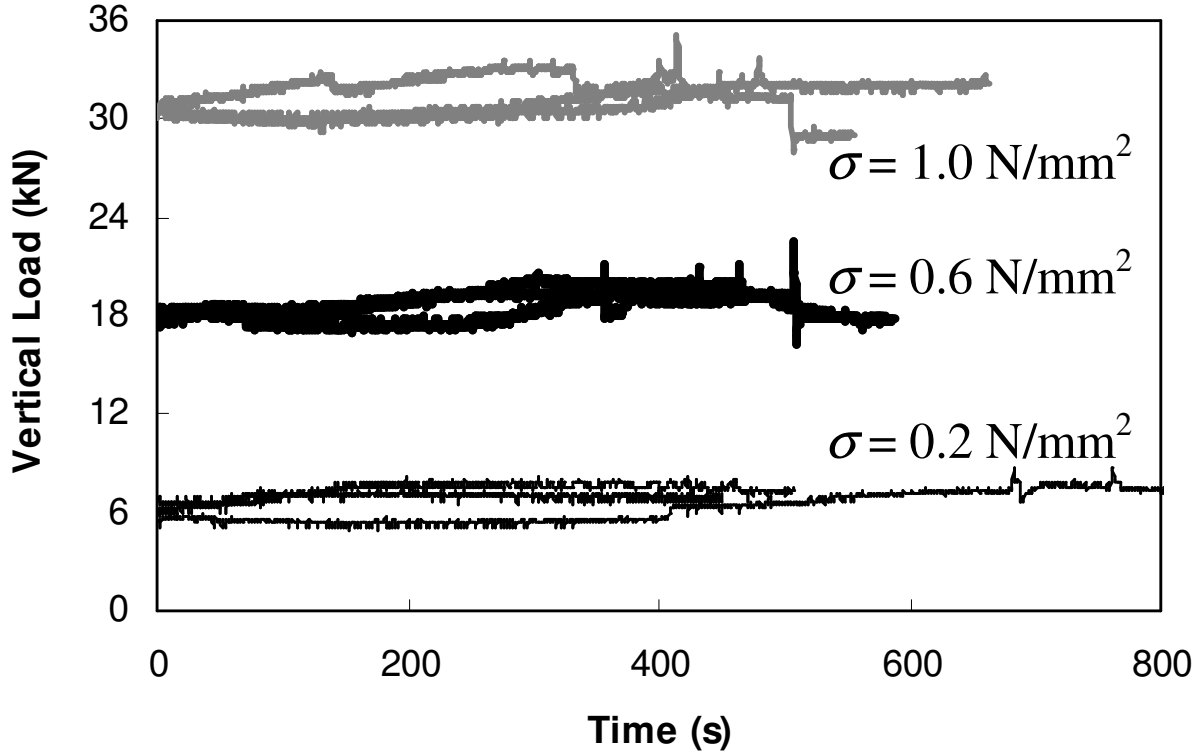

Figure 3 – Chronological history of the vertical load applied to panels under force control (σ is the pre-compression level).

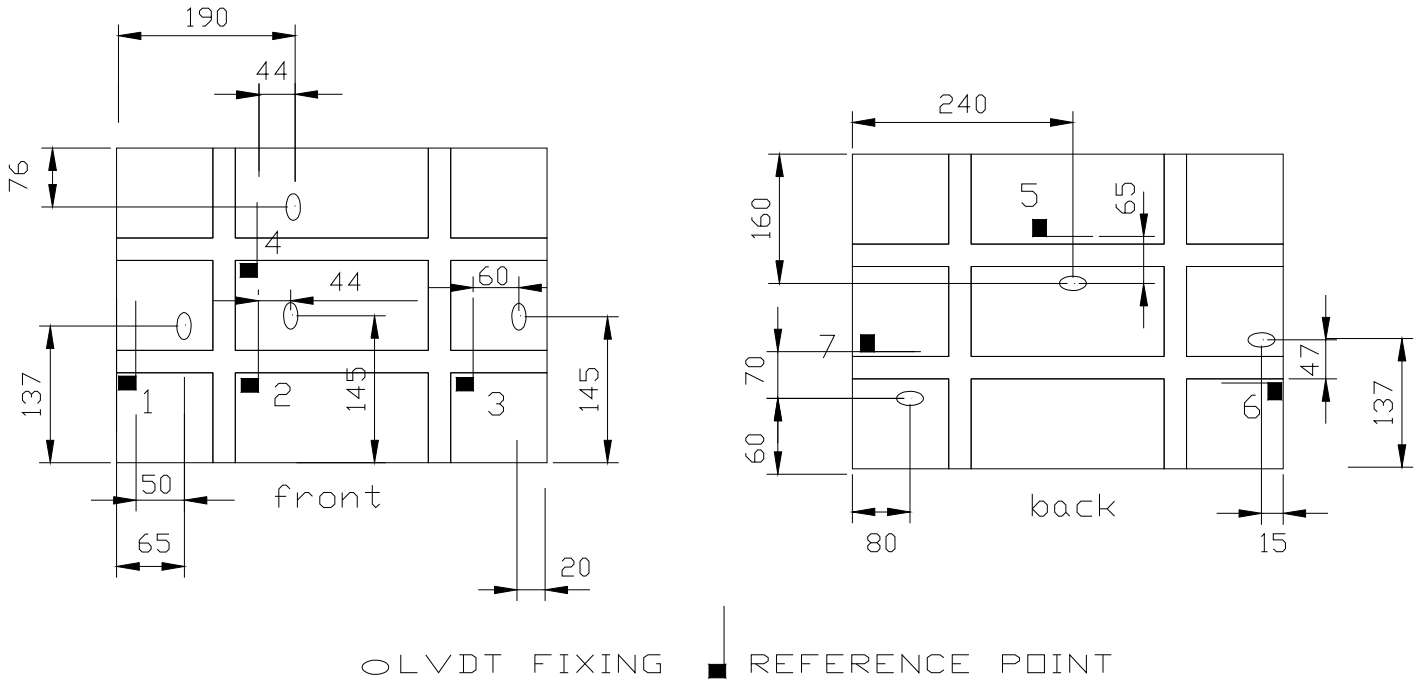

Figure 4 – Location of LVDTs in the panels, with dimensions in mm

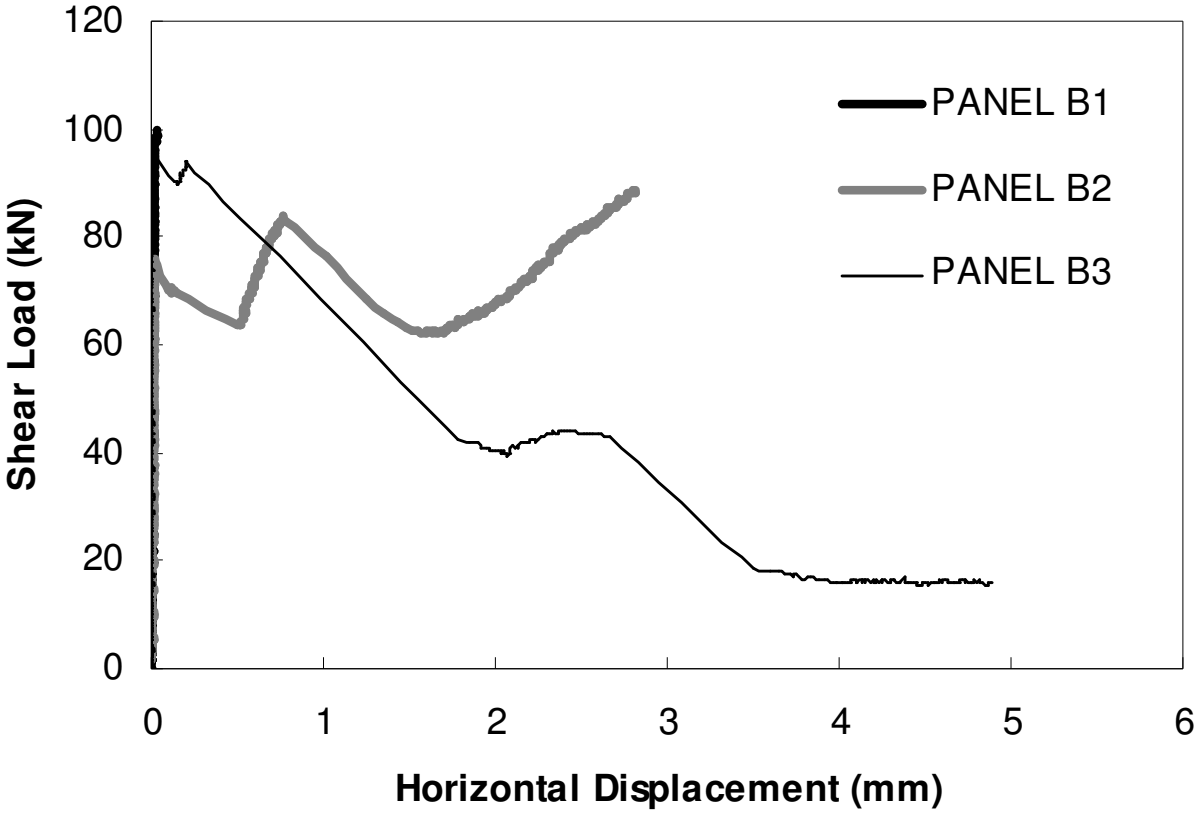

(a)

Figure 5 – Experimental results for series 1, in terms of: (a) shear load vs. horizontal displacement; (b) relation between the horizontal displacements of the top and bottom joints

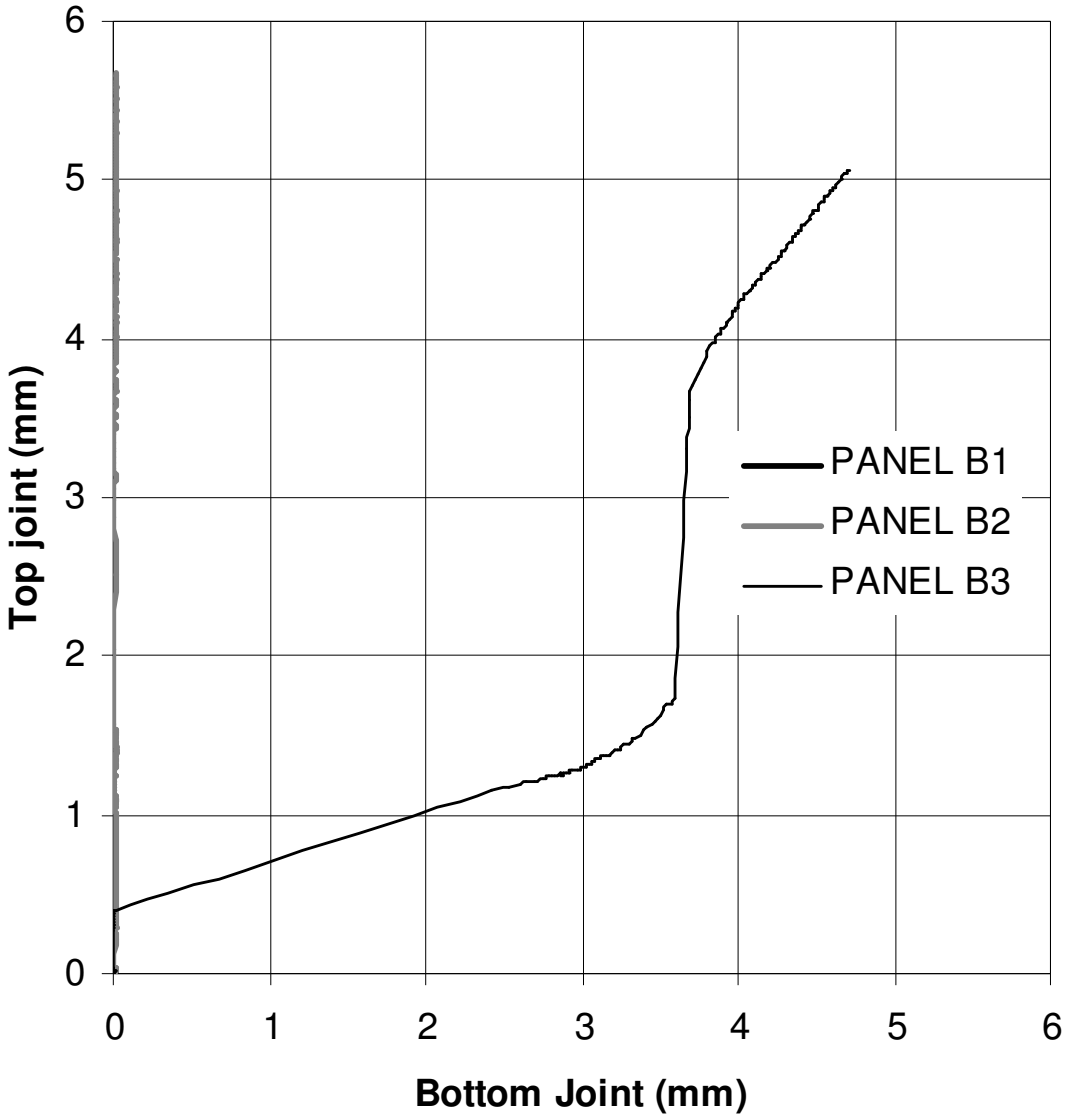

(b)

Figure 5 – Experimental results for series 1, in terms of: (a) shear load vs. horizontal displacement; (b) relation between the horizontal displacements of the top and bottom joints

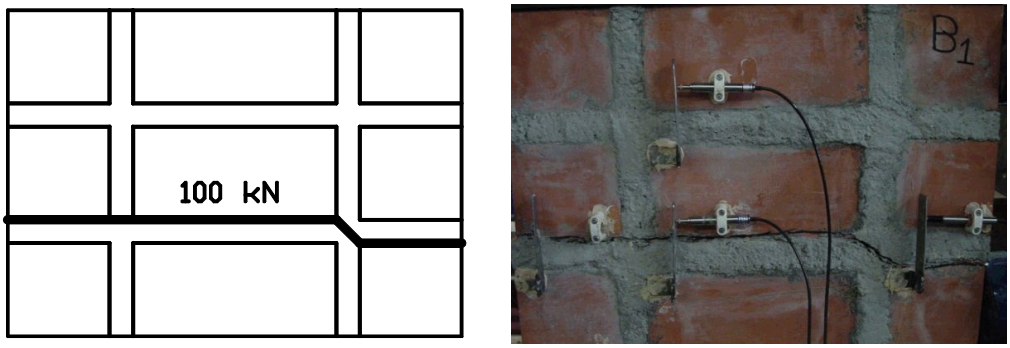

(a)

Figure 6 – Failure mode of the panels for series 1: (a) Panel 1; (b) Panel 2; (c) Panel 3.

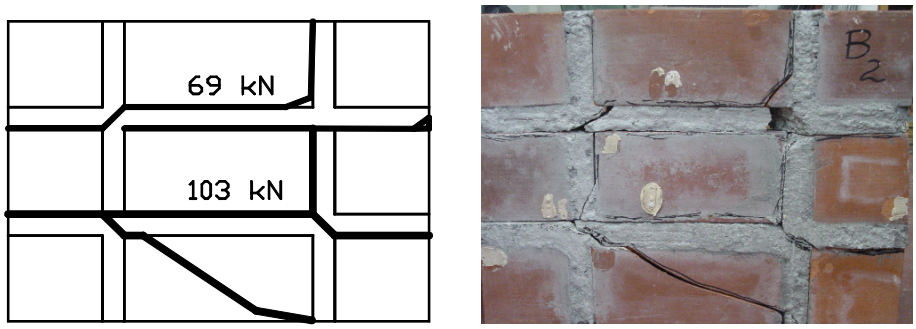

(b)

Figure 6 – Failure mode of the panels for series 1: (a) Panel 1; (b) Panel 2; (c) Panel 3.

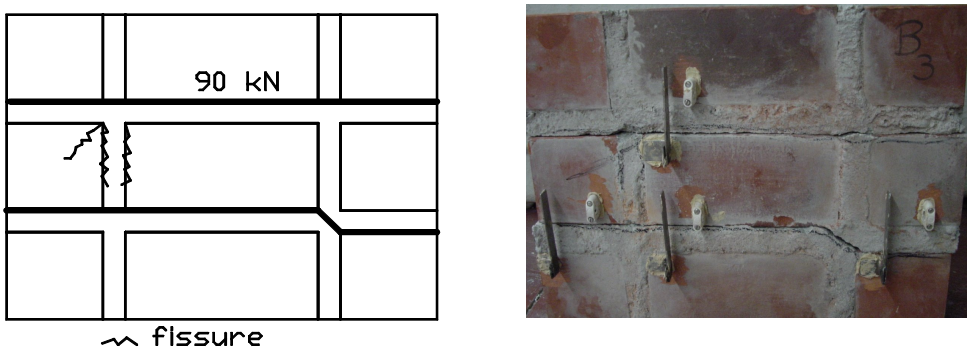

(c)

Figure 6 – Failure mode of the panels for series 1: (a) Panel 1; (b) Panel 2; (c) Panel 3.

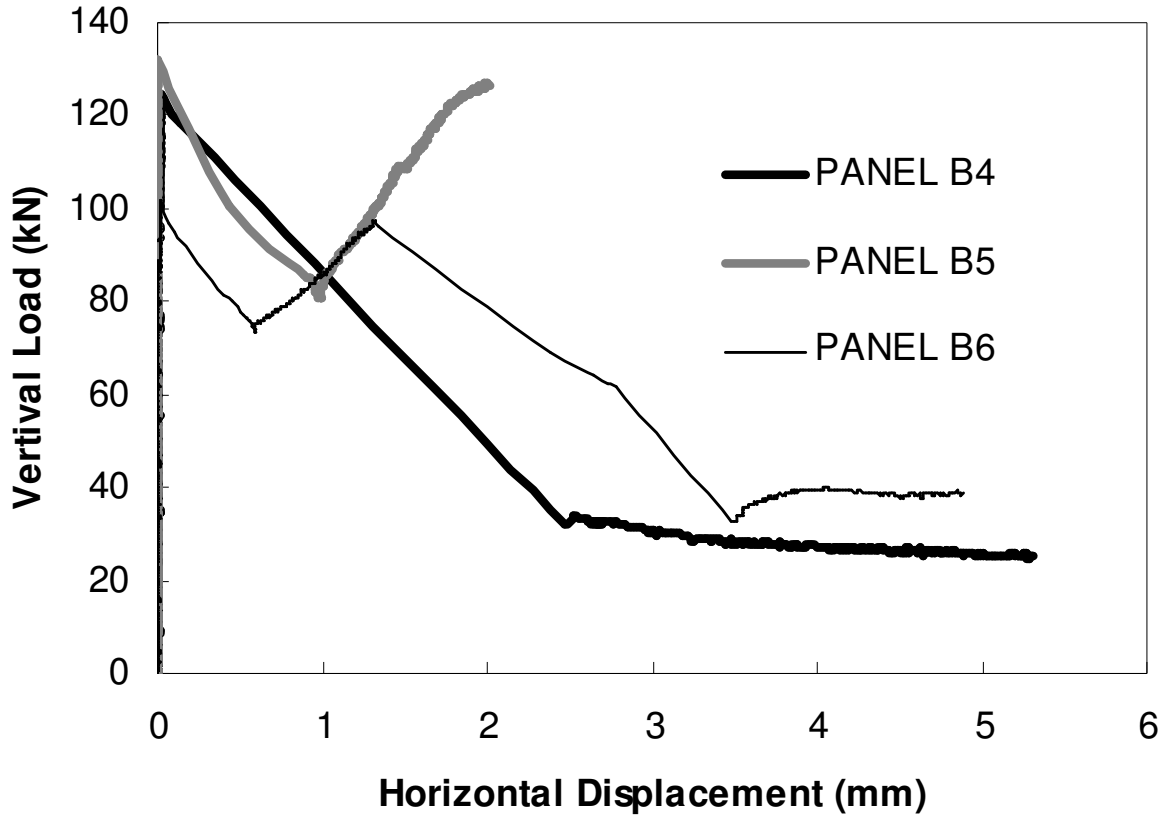

(a)

Figure 7 – Experimental results for series 2, in terms of: (a) shear load vs. horizontal displacement; (b) relation between the horizontal displacements of the top and bottom joints

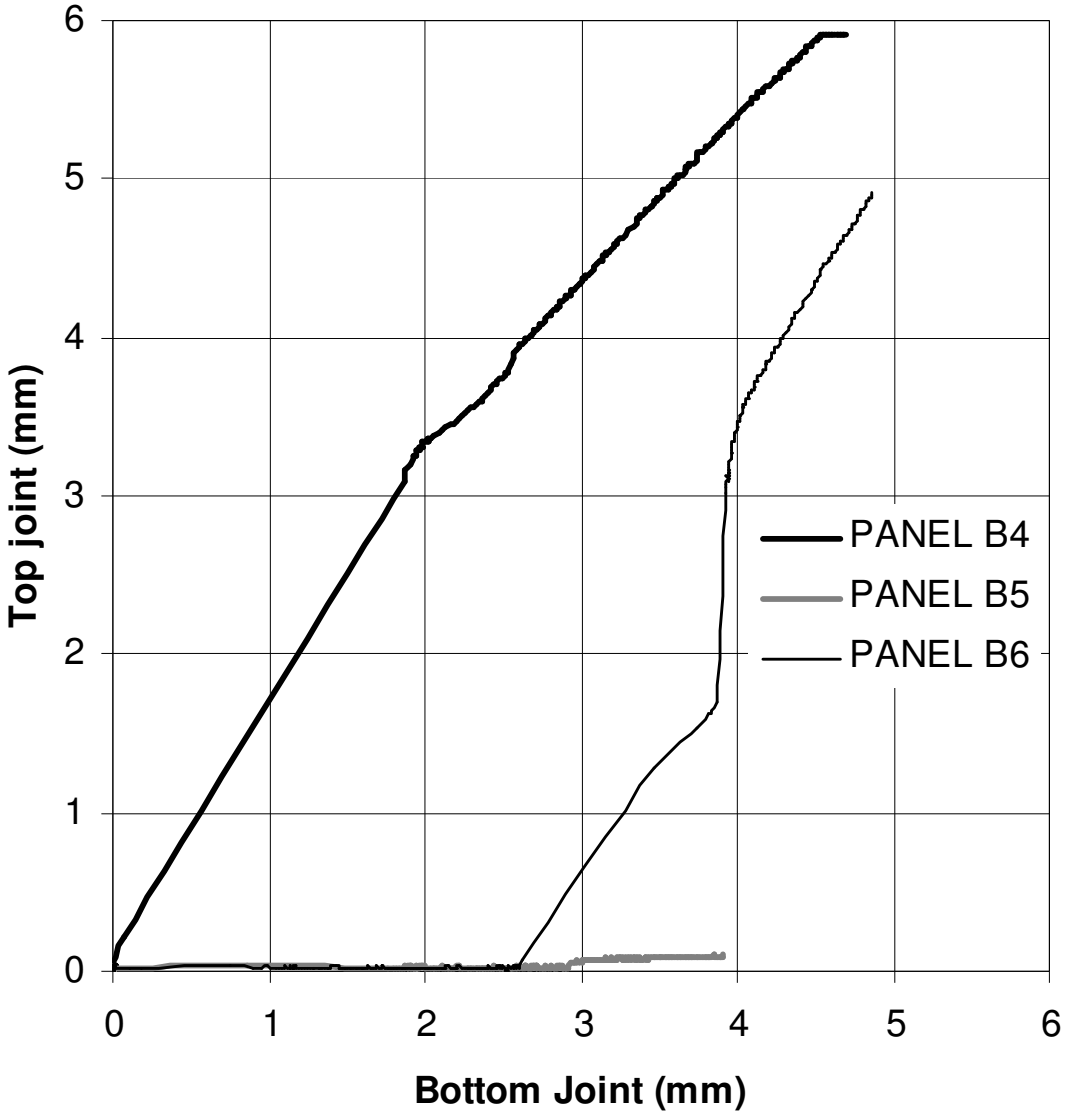

(b)

Figure 7 – Experimental results for series 2, in terms of: (a) shear load vs. horizontal displacement; (b) relation between the horizontal displacements of the top and bottom joints

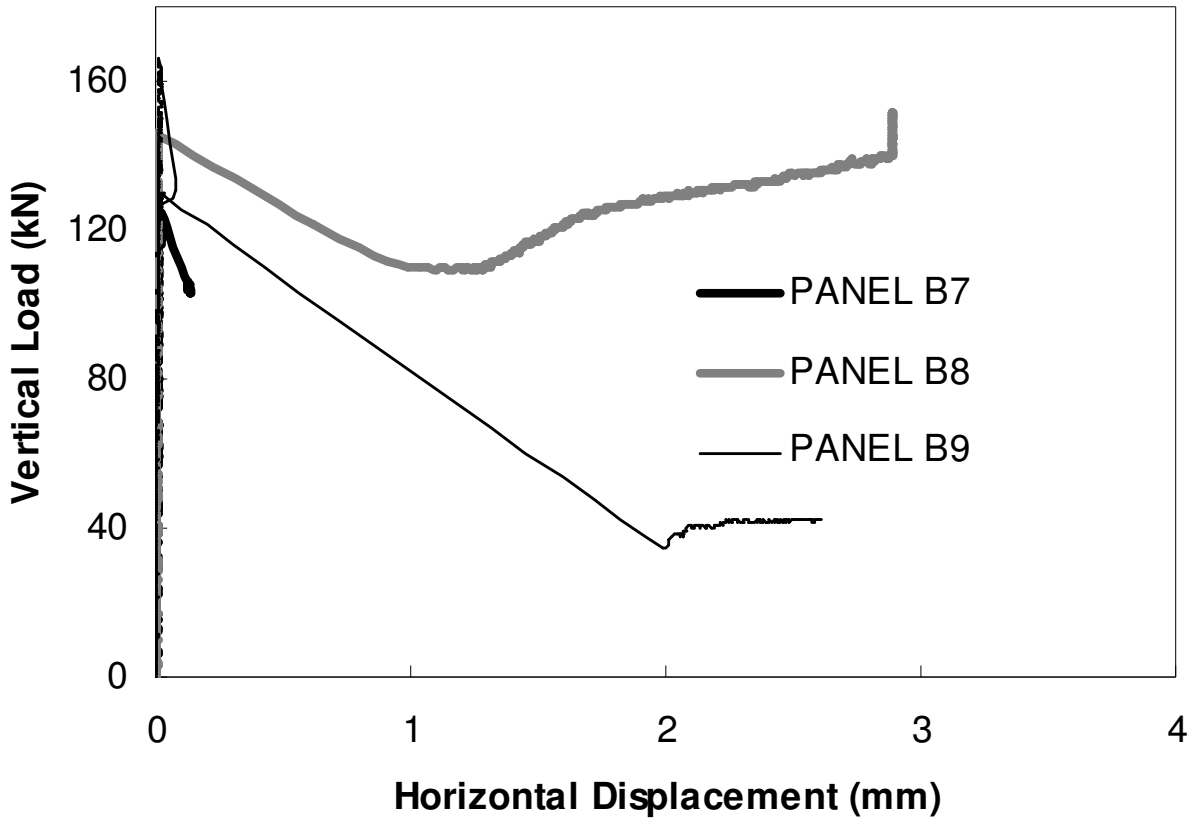

(a)

Figure 8 – Experimental results for series 3, in terms of: (a) shear load vs. horizontal displacement; (b) relation between the horizontal displacements of the top and bottom joints

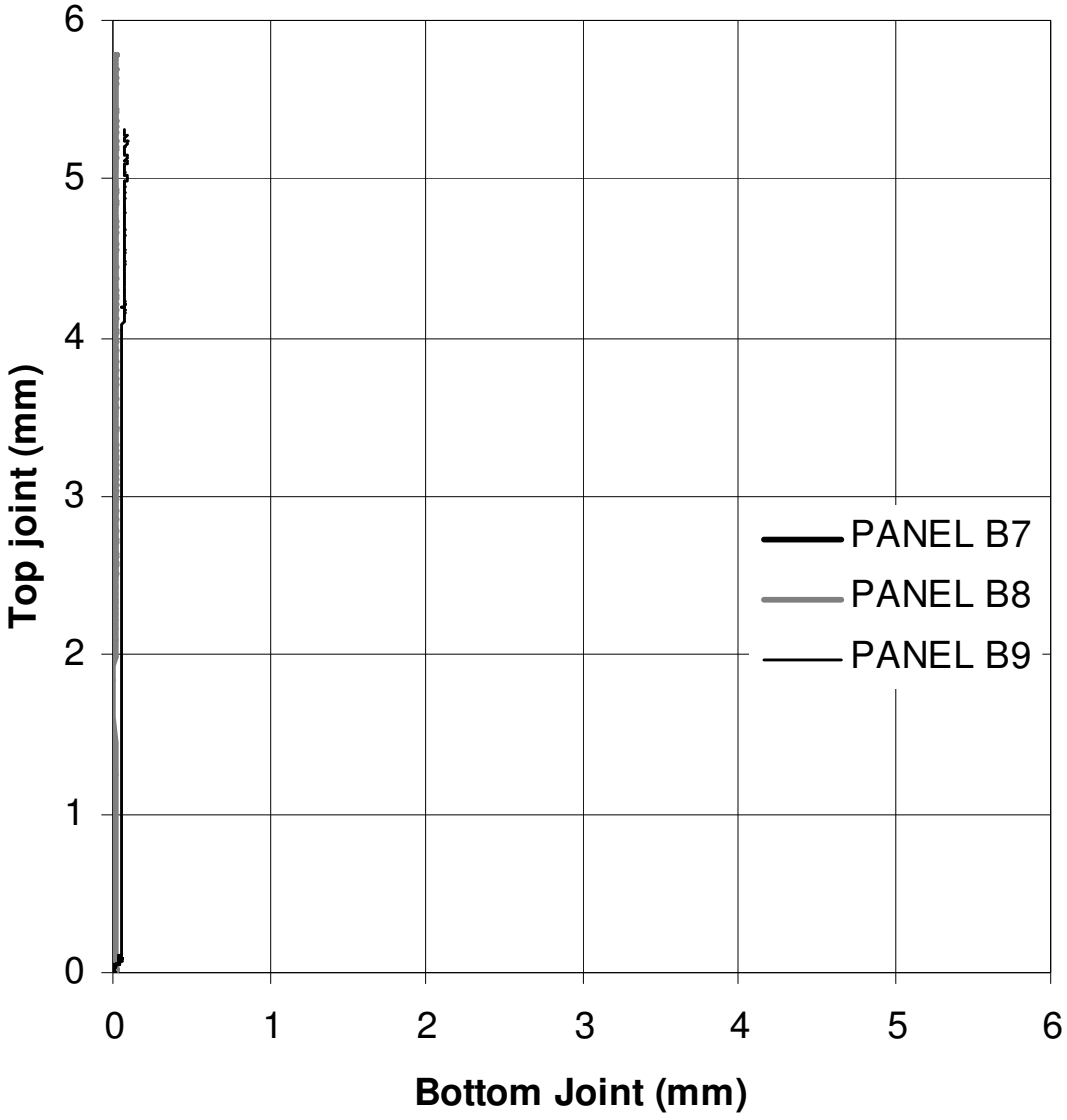

(b)

Figure 8 – Experimental results for series 3, in terms of: (a) shear load vs. horizontal displacement; (b) relation between the horizontal displacements of the top and bottom joints

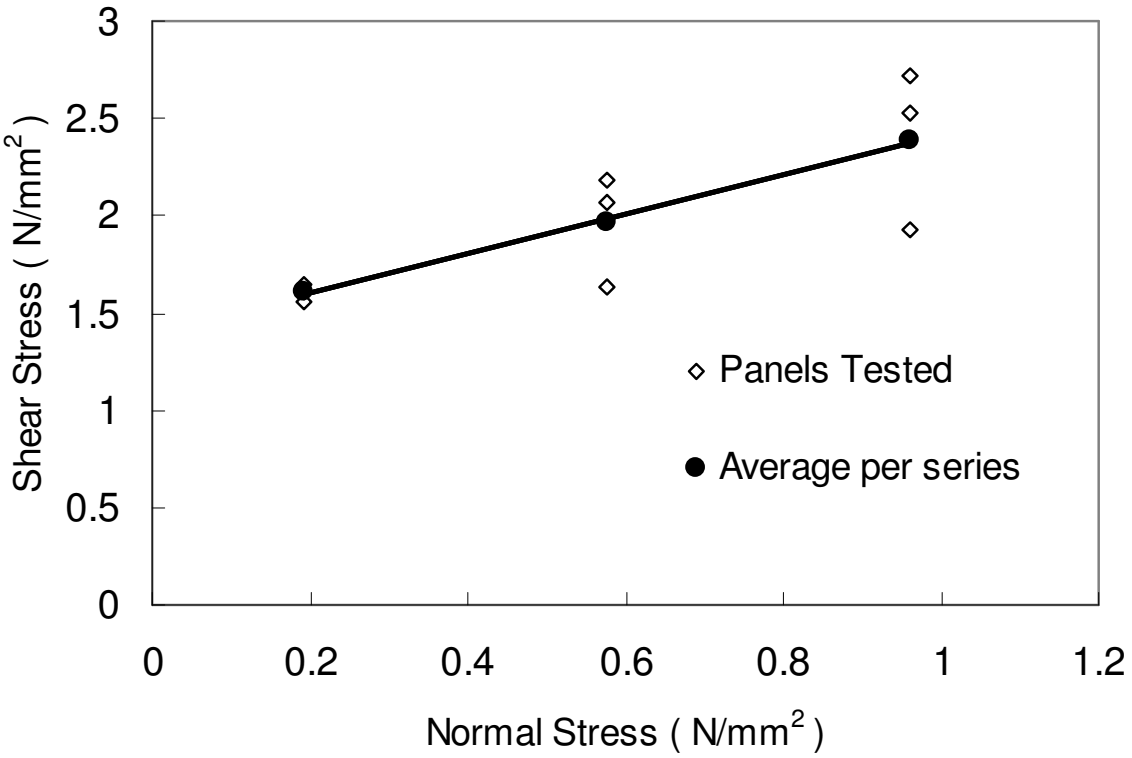

Figure 9 – Relation between shear strength and normal stress

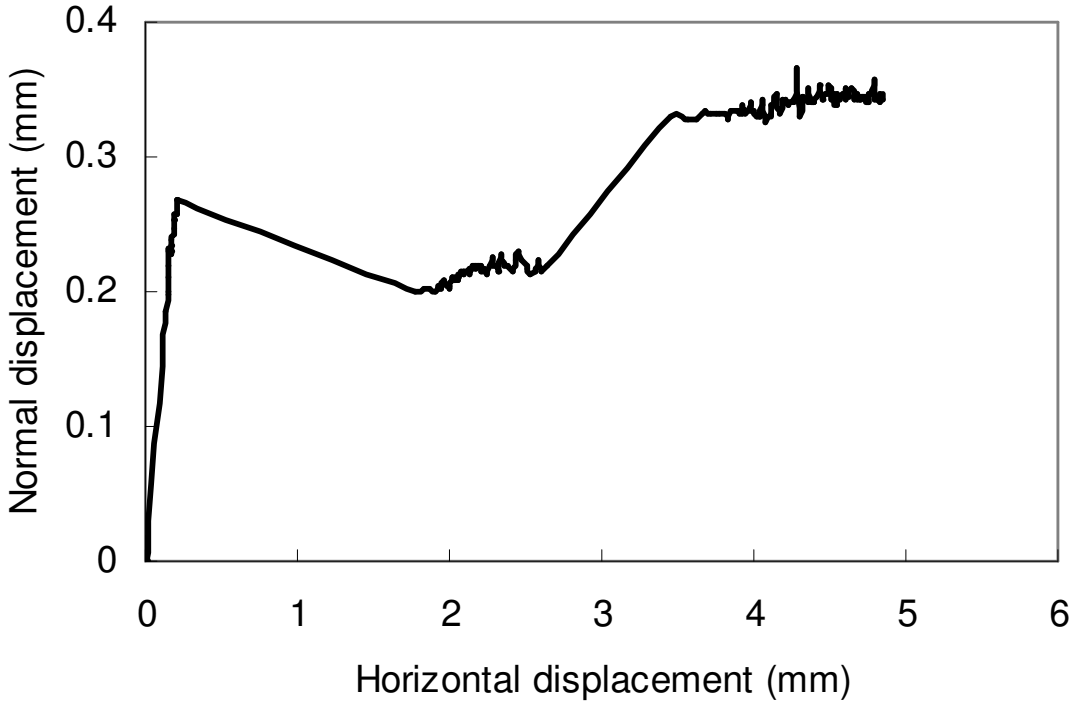

Figure 10 – Relation between horizontal and normal displacement, for panel B3